High Energy Density Physics 10 (2014) 9–15

Contents lists available at ScienceDirect

High Energy Density Physics

journal homepage: www.elsevier.com/locate/hedp

Molecular dynamics simulations of shock-induced plasticity in tantalum

Diego Tramontina [a,b], Paul Erhart [c,k], Timothy Germann [d], James Hawreliak [c], Andrew Higginbotham [e], Nigel Park [f], Ramón Ravelo [d,g], Alexander Stukowski [h], Mathew Suggit [e], Yizhe Tang [i], Justin Wark [e], Eduardo Bringa [b,j,*]

[a] Agencia Nacional de Promoción Científica y Tecnológica, CABA, C1054AAH, Argentina
[b] Instituto de Ciencias Básicas, Universidad Nacional de Cuyo, Mendoza M5502JMA, Argentina
[c] Lawrence Livermore National Laboratory, Livermore, CA 94550, USA
[d] Los Alamos National Laboratory, Los Alamos, NM 87545, USA
[e] Department of Physics, Clarendon Laboratory, University of Oxford, Parks Road, Oxford OX1 3PU, UK
[f] Materials Modeling Group, AWE, Aldermaston, Reading, Berkshire RG7 4PR, UK
[g] Physics Department and Materials Research Institute, University of Texas, El Paso, TX 79968, USA
[h] Darmstadt University of Technology, Darmstadt 64289, Germany
[i] Johns Hopkins University, Baltimore, MD 21218, USA
[j] Consejo Nacional de Investigaciones Científicas y Técnicas, Argentina
[k] Chalmer University of Technology, Department of Applied Physics, Gothenburg 41296, Sweden

ARTICLE INFO

Article history:
Received 10 October 2013
Accepted 16 October 2013
Available online 31 October 2013

Keywords:
Tantalum
Molecular dynamics
Shocks

ABSTRACT

We present Non-Equilibrium Molecular Dynamics (NEMD) simulations of shock wave compression along the [001] direction in monocrystalline Tantalum, including pre-existing defects which act as dislocation sources. We use a new Embedded Atom Model (EAM) potential and study the nucleation and evolution of dislocations as a function of shock pressure and loading rise time. We find that the flow stress and dislocation density behind the shock front depend on strain rate. We find excellent agreement with recent experimental results on strength and recovered microstructure, which goes from dislocations to a mixture of dislocations and twins, to twinning dominated response, as the shock pressure increases.
© 2013 Elsevier B.V. All rights reserved.

1. Introduction

Shock compression of condensed matter allows the study of materials under extreme conditions [1]. Improving experimental and simulation techniques allow detailed studies of the shock-induced microstructure, which can lead to large changes in mechanical properties. A large amount of work has been recently carried out for Face-Centered Cubic Metals (FCC) [2–13], and Body-Centered Cubic metals (BCC) [2,14–20]. However, most of the work on BCC metals has focused on Fe, due to the large number of technological applications for Fe, for instance as part of structural materials, and also due to the role of Fe properties in Earth's interior mechanics. Fe displays a solid–solid phase transformation near 15 GPa, which makes dislocation plasticity difficult to identify in simulations [21–23].

Atomistic simulations of high strain rate loading of BCC metals [3,24–26] are sparse, mostly due to the lack of interatomic potentials which are reliable at high pressures. In particular, it has been shown for Nb [18] and Ta [27], that many potentials display an artificial phase transition from BCC to Hexagonal Close-Packed (HCP).

Among BCC metals, Ta has several technological applications, and no phase transitions are thermodynamically present up to fairly high pressures and temperatures [28]. Shock-loaded Ta has been studied using both gas-gun [29] and laser-driven shocks [30–32]. These experiments show a rich behavior, including high strength [32,33], dislocations [29–31], twinning above a critical pressure around 40 GPa [30,31,34,35], and the presence of ω-phase [30,31] in some recovered samples shocked above ~70 GPa.

Recent Non-Equilibrium Molecular Dynamics (NEMD) simulations from Cuesta-Lopez and Perlado [36] subjected Ta, W and Fe monocrystals to particle velocities U_p ranging from 0.1 to 2.5 km s^{-1}, spanning the elastic to shock-melting response. They did not observe dislocation activity, but instead found nucleation

* Corresponding author. Instituto de Ciencias Básicas, Universidad Nacional de Cuyo, Mendoza M5502JMA, Argentina.
E-mail address: ebringa@yahoo.com (E. Bringa).
URL: http://sites.google.com/site/simafweb/

1574-1818/$ – see front matter © 2013 Elsevier B.V. All rights reserved.
http://dx.doi.org/10.1016/j.hedp.2013.10.007

of a close-packed phase above a critical shock pressure. However, this observed BCC → close-packed phase transition in Ta is actually an artifact of the potential by Li et al. [37] used in their study. Another group recently reported NEMD simulations of Ta spall [38], using the Johnson Embedded Atom Model (EAM) potential [39], without focusing on shock-induced plasticity.

Ravelo et al. recently presented a new EAM potential [27] for Ta specifically developed for high-pressure shock loading environments. They showed that several often-used Ta potentials display an artificial BCC → HCP transition below 100 GPa. Using their new potential, they calculated the Hugoniot along different directions: [001, 011] and [111], finding an excellent agreement with experimental data up to several Mbars. Above a velocity threshold ($U_p = 0.88$ km s^{-1}, P ~ 70 GPa for the [001] direction) they observed homogeneous nucleation of twins for shocks along all the studied directions. Above that threshold dislocations could be nucleated from twin boundaries. Rudd et al. [25] studied the plastic relaxation rates of compressed Ta samples, using the Model Generalized Pseudopotential Theory (MGPT) potential and homogeneous compression, finding dislocations homogeneously nucleated above ~65 GPa.

In this work we investigate a Ta sample with pre-existing defects which act as dislocation sources, shock loaded along the [001] crystallographic direction. We focus on pressures below 70 GPa, the threshold for twin nucleation, to study the influence of shock strength (particle velocity U_p) and shock rise time t_r on the resulting microstructures.

2. Methodology

We use the LAMMPS molecular dynamics simulation code [40], to model perfect single crystal samples, in which nanovoids have been added to act as dislocation sources [10,41–44]. A few nanovoids can be simple to introduce and relax, and have been extensively studied regarding dislocation emission under loading [15,25,45–47]. They lead to results similar to the introduction of dislocation loops [44,48], and have an activation stress roughly proportional to the inverse of their radius, compared to dislocation loop Frank-Read-type sources, which have a nucleation stress proportional to the inverse of their length [49]. We use nanovoids with a radius of 3 nm, which leads to an activation stress of 12 GPa under homogeneous uniaxial compression [50]. This allows us to study shock-plasticity well below the homogeneous twin nucleation limit.

We use the new EAM potential by Ravelo et al. [27], and the Extended Finnis Sinclair (EFS) potential [51]. These potentials should work well below 70 GPa, and dislocation activity from voids is qualitatively similar for both of them [50].

We tested different sample sizes, with cross-sections reaching 300 × 300 BCC cells to investigate possible size effects, and found that a cross-section of 50 × 50 cells was large enough to obtain smooth shock profiles. The length of the sample varied between 400 and 2000 BCC cells along the [001] direction. Periodic boundary conditions are applied in the transverse directions, and the back region allows for free surface release. Most simulations were run at low temperatures (10 K) to simplify defect detection, but the few room temperature simulations performed also displayed the same behavior.

There are several ways to run non-equilibrium shock simulations [4,52,53], and we use a simple rigid piston moving at an imposed particle velocity U_p [54,55]. An ideal shock wave is typically applied as a perfect square wave, with zero rise time. Experimental shocks, on the other hand, are typically applied with rise times as long as a nanosecond. For this reason, we use a linear velocity ramp for the piston, which can lead to a large change in the resulting microstructure due to the dynamics of dislocation production in the pre-existing sources [48,56]. Of course, the shock wave will eventually develop a steady state depending on pressure and material properties. We investigate piston velocities in the range $U_p = 0.25$–0.9 km s^{-1}, and rise times in the range $t_r = 0.1$–50 ps. As a guide, the volumetric compression reached for $U_p = 0.75$ km s^{-1} is 12%.

The deviatoric shear stress was calculated using [4]:

$$\sigma_1 = \frac{1}{2}\left(s_{zz} - \frac{1}{2}\left(s_{xx} + s_{yy}\right)\right); \tag{1}$$

while for the full von Mises stress we use:

$$\sigma_{vm}^2 = 3J_2 = \frac{1}{2}S_n + 6S_s; \tag{2}$$

$$S_n = \left(s_{xx} - s_{yy}\right)^2 + \left(s_{yy} - s_{zz}\right)^2 + \left(s_{xx} - s_{zz}\right)^2; \tag{3a}$$

$$S_s = s_{xy}^2 + s_{yz}^2 + s_{xz}^2; \tag{3b}$$

where J_2 is the second invariant of the stress deviator [13].

Tracking of defects was performed by use of the Dislocation Extraction Algorithm (DXA) [57]. In the DXA, defects are identified via Common Neighbor Analysis (CNA) [58] and a geometric description of dislocation lines is generated. All remaining crystal defects which cannot be represented by dislocation lines are identified as point defects or surfaces, which in our specific case would apply for vacancies, twin boundaries, or void surfaces. This geometric representation is ideal for visualization of complex defect structures. We also used the Crystal Analysis Tool (CAT) [59], which allows for strain and structure-type calculations, including twin detection. Although twin identification in unstrained lattices is fairly straightforward using CNA or other methods [60], twinning in a lattice with large uniaxial compression can be challenging. CAT [59] is able to detect twins up to high strains, and a new method for twin identification has also been recently presented [61]. We use Ovito [62], VMD [63], and ParaView [64] to visualize defect structures.

3. Results

Shock loading leads to emission of dislocations from pre-existing sources, as expected. Initially, as described in detail for homogeneous loading simulations [46], one observes mostly rapid edge segments advancing while screw segments remain mostly sessile, as shown in Fig. 1a, for $U_p = 0.35$ km s^{-1}, $t_r = 15$ ps. Shock simulations using the EFS interatomic potential by Dai et al. [51] show the same features. Although there are some quantitative differences in the activation threshold for dislocation emission between the EFS and Ravelo potentials, dislocation structures for 3 nm voids are qualitatively the same under homogeneous compression [50]. After some time, a dislocation forest develops, as in the back of Fig. 1a, similar to the case of higher porosity and homogeneous uniaxial loading [47], with a large fraction of straight screw segments, as seen in some recovered samples. For $U_p < 0.4$ km s^{-1} (29 GPa), only dislocations are nucleated from the pre-existing defects, and the situation evolves similarly to Fig. 1a. For $U_p = 0.5$ km s^{-1}, twinning appears as shown in Fig. 1b. We find a twinning threshold between 25 and 30 GPa, in agreement with experiments [31]. Twinning appears alongside dislocations, producing a mixed structure as observed in Fig. 1b, obtained with CAT [59]. This has also been seen in gas-gun [65] and laser-driven shock experiments [31]. In our simulations twins are only few nm wide

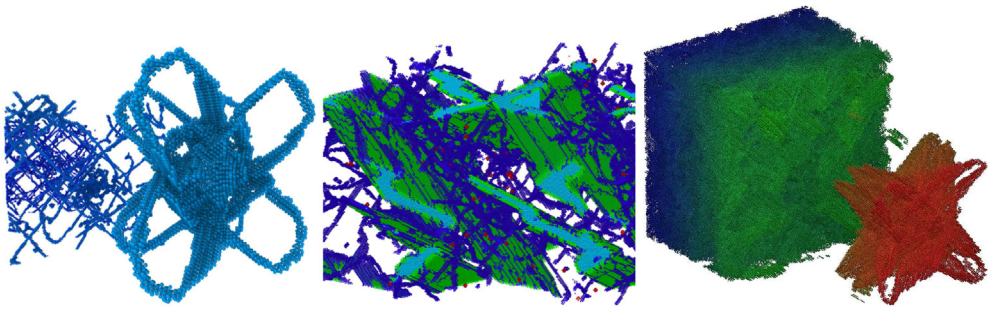

Fig. 1. Shock-induced microstructure for the Ravelo potential [27], with shock fronts moving approximately from left to right. (Left) $U_p = 0.35$ km s^{-1} and $t_r = 15$ ps, showing dislocations 60 ps after piston started. (Center) $U_p = 0.50$ km s^{-1} and $t_r = 15$ ps, showing twinning and dislocations, 70 ps after shock started. Blue: dislocations; teal: twins; green: twin boundaries. (Right) $U_p = 0.88$ km s^{-1}, $t_r = 15$ ps. Behind dislocations emitted from the void, twins are nucleated homogeneously. Color represents depth. (For interpretation of the references to color in this figure legend, the reader is referred to the web version of this article.)

and few tens of nm long after only 50–80 ps, and they could continue growing. The microscopy work by McNaney et al. showed that twins in recovered Ta (001) samples shocked at 55 GPa were tens of nm wide and hundreds of nm long [35]. Recent work for compressive loading of Ta at 10^4 s^{-1} also shows thin twins [66]. The case when the twin nucleation threshold has already been reached is shown in Fig. 1c. Since we are using ramp loading, the early part of the ramp is enough to trigger dislocation emission from a void, while the peak pressure reached at the top of the ramp induces twinning. This should be compared to the FCC loading shown in Refs. [48,56], where loops were used instead of voids, and homogeneous nucleation of shear loops replaced twinning.

Twinning in BCC metals is complex [67–69], but there are several atomistic studies for BCC metals describing twin growth [70,71], and twin nucleation from grain boundaries [72,73]. In our simulations, twinning is closely related to dislocation emission from voids and their reactions [46]. As expected from compressive strain, shock-induced twins are in the $(\bar{1}21)[11\bar{1}]$ system [46]; Fig. 2 shows the close-up view of a twin from the simulation shown in Fig. 1b.

A view of the shock-induced dislocation forest produced by a single source can be seen in Fig. 3, together with pressure and shear stress profiles. The von Mises stress has an average value of ~12 GPa over the region with dislocations, which is nearly identical to its value throughout the entire shock-compressed region. The shear stress goes down to values of 3 GPa, less than half its value in the elastically compressed region.

To understand the large differences between the von Mises and shear stress, we consider one particular case. In Fig. 5, the profiles for the longitudinal stress tensor component in the shock direction σ_{zz}, von Mises stress σ_{vm}, shear σ_1, and the orthogonal shear stresses σ_{xy}, σ_{xz} and σ_{yz} are plotted for a shocked sample at $U_p = 0.5$ km s^{-1} with a linear ramp of $t_r = 10$ ps. A void at $z \sim 66$ nm serves as a dislocation source. It can be seen that σ_{zz} maintains its value at ~36 GPa in the region with dislocations, between 55 and 90 nm, but we sometimes observe perturbations near voids, especially for longer rise-times. The von Mises stress has a mean value of 13 GPa with a drop of only about 5% near the center of the dislocation zone. On the other hand, as the shear stress is only computed from the principal stress directions, it shows a marked drop over the same region, where a particular complex state of stress evinced by the non-zero values of the non-diagonal shear stress components diminishes the ability of the von Mises calculation to reflect deviatoric stress relaxation due to dislocation motion.

Fig. 4 shows profiles for samples with 3 dislocation sources along their length. Pressure profiles show the expected steepening of the wave, and kinks in the profile indicate plastic activity. Dislocation activity increases with time and leads to a roughly homogeneous dislocation density. Shear profiles display increasing relaxation due to that dislocation motion, as expected.

Fig. 6a shows the evolution of dislocation density, von Mises and shear stress, versus U_p. Measurements for this figure were taken at the same depth, when the shock front is reaching the end of the sample. The dislocation density grows with increasing particle velocity U_p as expected. It increases linearly with U_p for rise times up to 15 ps, but when the ramp is as long as 35 ps and U_p is at 0.75 km s^{-1}, the dislocation density no longer follows this trend, but instead shows a lower value. At longer rise times, dislocation motion dominates dislocation emission, lowering the dislocation density needed to relax the volumetric strain Ref. [48]. The large

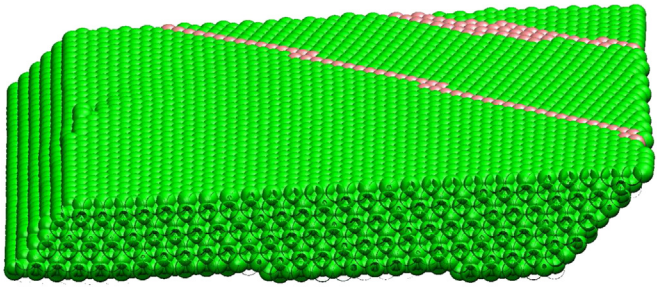

Fig. 2. Region of the sample, for $U_p = 0.50$ km s^{-1} and $t_r = 15$ ps, showing twinning induced by the pre-existing sources, below the homogeneous twin nucleation threshold, 70 ps after the shock started. Top surface perpendicular to the (112) plane.

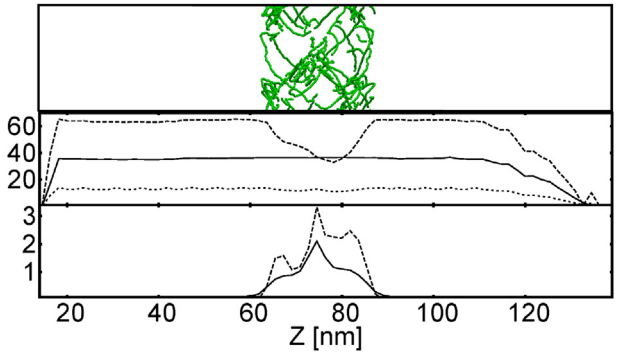

Fig. 3. Snapshot for $U_p = 0.50$ km s^{-1}, $t_r = 15$ ps, taken 35 ps after the piston started, for a sample with an initial void in the center. (top) Dislocation lines. (center) Longitudinal stress (solid line), shear stress (×10, dashed line) and von Mises stress (dotted line), all in GPa. (bottom) Temperature (×10^{-2} K, solid line), and dislocation density (×10^{-17} m^{-2} dashed line).

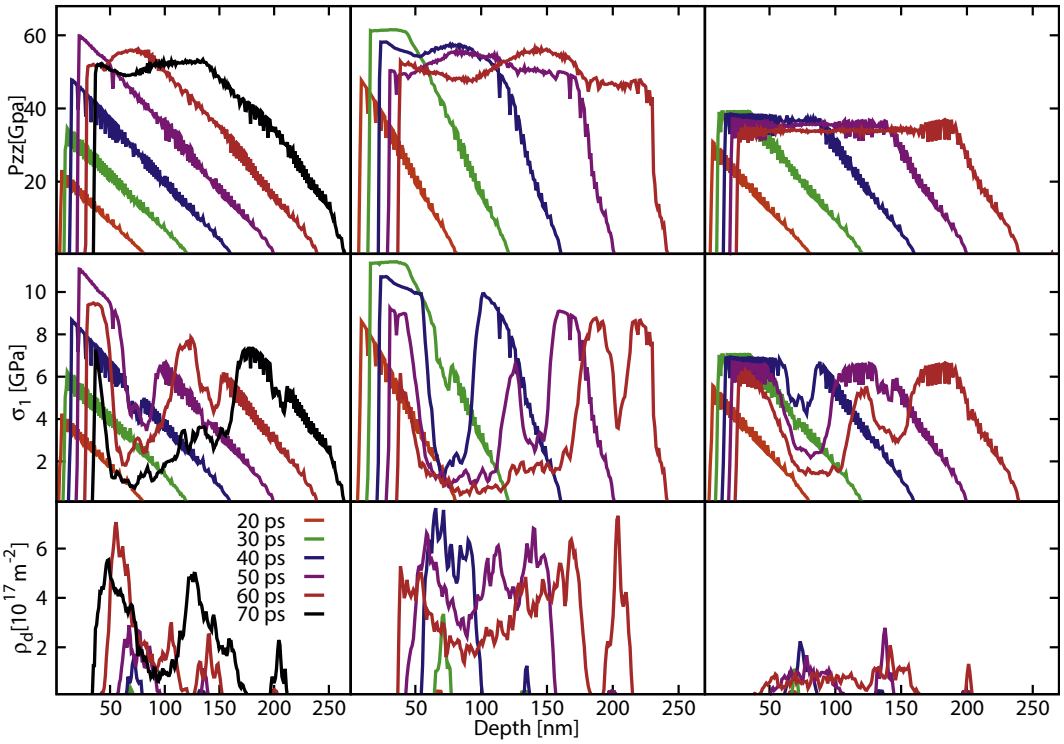

Fig. 4. Selected profiles at distinct shock velocities and rise times. First column: $U_p = 0.75$ km s^{-1}, $t_r = 50$ ps. Second column: $U_p = 0.75$ km s^{-1}, $t_r = 25$ ps. Third column: $U_p = 0.50$ km s^{-1}, $t_r = 25$ ps.

dislocation densities might be partly due to particularly large multiplication rates for (001) loading [34]. The von Mises stress depends weakly and the shear stress strongly on both U_p and t_r over the entire range shown here.

In Fig. 6b, the shear stress σ_1, von Mises stress σ_{vm} and dislocation density ρ_d have been plotted as a function of the simulation time in order to observe the evolution at distinct ramp times. In all cases, there is an initial rise stage up to a maximum value, followed by a decay at later times. All curves shown in this figure are for $U_p = 0.5$ km s^{-1}, so the maximum shear stress in this condition is about 12 ∼ 15 GPa. This is enough to trigger dislocation emission from pre-existing dislocation sources, and lead to relaxation of the shear stress [25,48]. As expected, the dislocation density is greatest for the shorter rise time.

The shear stress, von Mises stress, and dislocation density as a function of the rise time are shown in Fig. 7, for $U_p = 0.5$ km s^{-1}. Whereas the von Mises stress shows the same trend for all simulated rise times, the shear stress and dislocation density present a local minimum at $t_r = 5$ ps due to the competition between dislocation emission and motion. We note that dislocation densities go down to $\sim 10^{16}$ m^{-2} for the longest simulated rise time, as also shown in Fig. 4. The longest rise times presented here might still be shorter than typical experimental rise times, pointing to possible further reduction of transient dislocation densities in experiments.

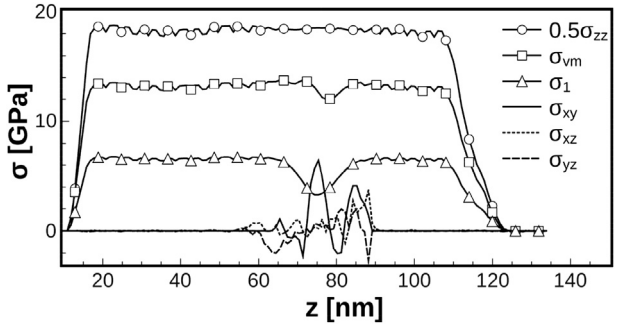

Fig. 5. Stress profiles at $t = 30$ ps, for $U_p = 0.5$ km s^{-1} and $t_r = 10$ ps. Shear differs depending of the criteria employed, specially in the dislocation zone, between 55 and 90 nm.

4. Discussion of results and comparison with experiments

Experimental single crystal metal samples always contain a level of pre-existing defects, including vacancies, impurities, dislocation loops, and dislocation networks. The amount and structure of these defects can determine the Hugoniot Elastic Limit (HEL) and the plastic shock response at low pressures. For instance, dislocation loops which are near micron-sized, as often found in experimental samples, would lead to dislocation multiplication at stresses of tens of kbars, as shown in FEM-DD (Finite Element Method-Dislocation Dynamics) of shocks in Ta [56]. The role of dislocation networks in shock plasticity is more difficult to asses. In atomistic simulations one is typically limited by dislocation sources with activation stresses above 1 GPa. Because of this, and the high strain-rate in shock compression, there is an immense production of dislocations, reaching densities of $\sim 10^{16}$–10^{17} m^{-2}. Similar densities are found in homogeneous compression of defective Ta samples [47], and are comparable to densities in shocked FCC metals [48,56,74]. The dislocation densities we find in our simulations are similar to the predictions of the Multi-Scale Strength (MTS) model, which predicts a saturation dislocation density of $\sim 10^{16}$ m^{-2} at a strain rate of 10^9 s^{-1} [75]. There are experiments where dislocation densities in shock-loaded and recovered Ta samples have been estimated to be larger than 10^{16} m^{-2} [65].

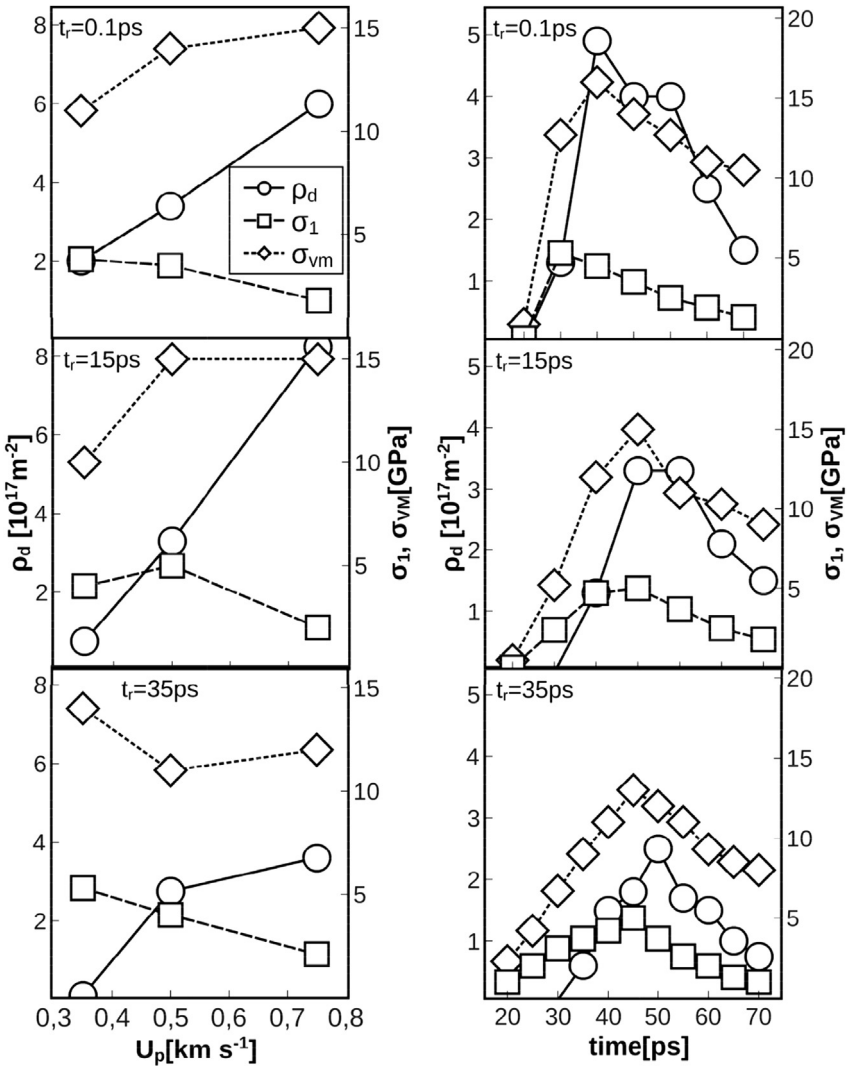

Fig. 6. (left) Evolution of local dislocation density, resolved shear stress and von Mises stress versus piston velocity, for selected rise times. Quantities are evaluated 60 nm ahead of the piston, when the shock wave is reaching the far back of the sample. (right) Same parameters evaluated as a function of time, for $U_p = 0.5$ km s^{-1}. Symbol size is indicative of error.

Lu et al. [31] discuss two semi-analytical models of dislocation production. One of them assumes homogeneous nucleation (HN) of dislocations, and another assumes dislocation emission from sources, sometimes referred as heterogeneous nucleation (HetN). The first one leads to dislocation densities of 10^{16}–10^{17} m^{-2}, and the second one leads to densities of $\sim 10^{14}$ m^{-2}. Dislocation densities in recovered samples were around 10^{14} m^{-2} and, therefore, it was concluded that HN was not relevant, but HetN was dominant. However, HN was suggested again to explain the results by Comley et al. [32] based on the simulations by Rudd et al. [25]. In this work, we found high dislocation densities due to source emission, and do not observe HN, neither in shocks nor in homogeneous uniaxial compression. We thus agree with Lu et al. [31] regarding the crucial role of HetN.

The large discrepancy between our simulated values and the ones reported by Lu et al. [31] could be explained by the difference between densities during loading and after recovery. For FCC metals, it was shown that there could be several orders of magnitude decrease between the two values [76]. For BCC metals one would expect that recovery might play a lesser role, due to reduced dislocation mobilities. However, preliminary results for simulated recovery show a dislocation density decrease by a factor of 10 within few tens of ps. This points to the possibility of further reduction of the dislocation density during macroscopic time scales. Recent experiments looking at perturbation growth during Ta loading [24], also suggest that the transient dislocation densities reached during loading are much larger than those found in recovered samples.

Hammel et al. [33] found flow stresses of 2–3 GPa for shocks in Ta up to 50 GPa, at a strain rate of 10^7 s^{-1}. Our simulations are carried out at higher strain rates, and a larger flow stress is expected. In fact, the values of strength in the simulations, as given by the von Mises stress, are consistent with X-Ray Diffraction-based observations of Ta strength obtained by Comley et al. [32] at similar pressures and strain rates. This would also support the large dislocation densities we find in our simulations during loading.

Based on our results, one could distinguish three different regimes in the shock-induced microstructure. At relatively low pressures there are only dislocations, which upon recovery would arrange into dislocation cells. Above 30 GPa there is a mixture of dislocations and twins, up to ~70 GPa, when massive twin nucleation would dominate the resulting microstructure. This

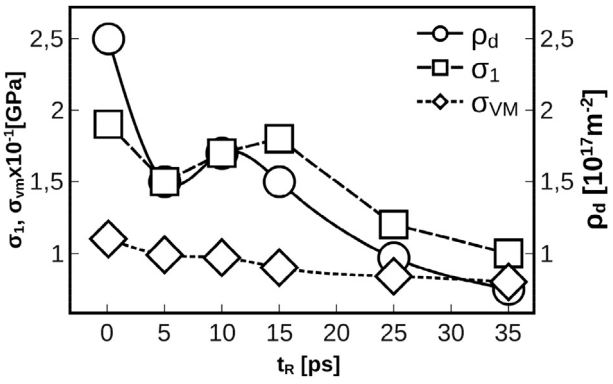

Fig. 7. Dislocation density, shear and von Mises profiles versus rise time, for $U_p = 0.5$ km s^{-1}. Symbol size is indicative of error.

hierarchy of shock-induced microstructures agrees very well with experimental results by Hsiung [65] and Lu [31]. The work by Florando et al. [34] for shocks in Ta (001) showed twin fractions in recovered samples which are negligible for 25 GPa shocks, and of up to few percent for 55 GPa shocks. We have 0% twin volume fraction in Fig. 1a, for 25 GPa shocks ($U_p = 0.35$ km s^{-1}), 3.5% twin volume fraction in Fig. 1b, for 37 GPa shocks ($U_p = 0.5$ km s^{-1}); and 6% twin volume fraction in Fig. 1c, for 67 GPa shocks ($U_p = 0.88$ km s^{-1}).

These results point out the need for constitutive models that include twinning, as the ones recently presented for HCP [77] and BCC metals [34,78]. The recent MTS model by Barton et al. [75], which agrees well with experimental strength up to 200 GPa [32] only includes dislocation plasticity. Therefore, its applicability to monocrystals shocked above ~50 GPa, where recovered samples and simulations display twinning, should be taken with care, as the authors themselves point out. The newly presented constitutive model by Florando et al. [34] includes both slip and twinning and reproduces trends seen in experiments for Ta single crystals. It contains dislocation slip as MTS, and focuses on twin growth and interaction between slip and twinning, without including twin nucleation explicitly. In our simulations, twins are nucleated near dislocation sources, and the twinning fractions we find are consistent with results from this new model.

Regarding the nucleation of the ω-phase seen in recovered samples [31,65], we do not find evidence of such nucleation in our loading simulations, but phase-stability studies are in progress for the interatomic potentials used here. It could certainly happen that the kinetics of ω-phase nucleation is much longer than the ~100 ps scale covered in our simulations, or that recovery plays a role in the formation of the omega phase.

5. Summary and conclusions

Molecular Dynamics simulations of shocks in (001) Ta single crystals with pre-existing defects show dislocation and twin production, which lead to shear stress relaxation. Stress relaxation is less noticeable if one uses the von Mises stress, because the off-diagonal stress components increase the values of the shear stress. Dislocation densities and flow stress decrease with increasing rise time of the applied load. The simulated Ta strength agrees well with recent experimental values [32].

Shock-induced microstructure consists of dislocations at relatively low pressures, followed by a combination of dislocations and twins starting at ~30 GPa, and finally a predominance of twins above 70 GPa. This succession of microstructures and the shock pressures at which they occur agree well with experimental results [31,34]. However, we find dislocation densities which are much higher than the ones in recovered samples [31], which could be explained by experimental unloading and recovery during macroscopic time. At the end of our loading simulations we typically observe a dislocation forest with a large fraction of screw segments. Recovered samples also include many screw segments, along dislocation loops and dislocation cells [31]. However, it is difficult to compare our dislocation structure during loading to structures generated after unloading and long thermal processing. Dynamic diffraction experiments might offer a window to study dislocation plasticity during loading [48,79].

There are several aspects of simulations of shocks in Ta single crystals which need to be explored further. For instance, shocks in single crystals with different orientation such as [011], analysis of twinning [59,61], detailed elastic–plastic strain calculations [59], together with simulated diffraction patterns which will allow a direct comparison with experimental results [32,48,61,79]. Shocks in Ta polycrystals would also offer rich microstructures.

Plasticity in Ta offers a scenario to test our knowledge of the behavior of solids at high strain rates. The increasingly better studies of microstructure evolution during and after shock loading will lead to improved understanding of materials performance, and the possible design of improved materials for use under extreme conditions [80].

Acknowledgements

D. Tramontina and E.M. Bringa were funded by projects PICT2008-1325 from the ANCyT and 06/M035 from SecTyP-U.N. Cuyo. We thank R. Rudd, B. Remington, M.A. Meyers, B.L. Holian and C.J. Ruestes for useful and stimulating discussions. A. Higginbotham acknowledges support from AWE. M. Suggit and J.S. Wark acknowledge support from EPSRC under grant P/J017256/1. R. Ravelo acknowledges support from the Air Force Office of Scientific Research under Award FA9550-12-1-0476. Work at Los Alamos was performed under the auspices of the U.S. Department of Energy (DOE) under Contract No. DE-AC52-06NA25396. P. Erhart acknowledges support from the Swedish Research Council (VR) and the Area of Advanced Materials at Chalmers.

References

[1] E. Gamaly, Phys. Rep. 508 (4) (2011) 91, http://dx.doi.org/10.1016/j.physrep.2011.07.002.
[2] M.A. Meyers, C. Taylor Aimone, Prog. Mater. Sci. 28 (1) (1983) 1, http://dx.doi.org/10.1016/0079-6425(83)90003-8.
[3] B.A. Remington, P. Allen, E.M. Bringa, J. Hawreliak, D. Ho, K.T. Lorenz, H. Lorenzana, J.M. McNaney, M.A. Meyers, S.W. Pollaine, K. Rosolankova, B. Sadik, M.S. Schneider, D. Swift, J. Wark, B. Yaakobi, Mater. Sci. Technol. 22 (4) (2006) 474, http://dx.doi.org/10.1179/174328406X91069.
[4] B.L. Holian, Science 280 (5372) (1998) 2085, http://dx.doi.org/10.1126/science.280.5372.2085.
[5] R.W. Armstrong, S.M. Walley, Int. Mater. Rev. 53 (3) (2008) 105, http://dx.doi.org/10.1179/174328008X277795.
[6] M.A. Meyers, H. Jarmakani, E.M. Bringa, B.A. Remington, in: J.P. Hirth, L. Kubin (Eds.), Dislocations in Solids, Elsevier, 2009, pp. 91–197, http://dx.doi.org/10.1016/S1572-4859(09)01502-2.
[7] V. Lubarda, M. Schneider, D. Kalantar, B. Remington, M. Meyers, Acta Mater. 52 (6) (2004) 1397, http://dx.doi.org/10.1016/j.actamat.2003.11.022.
[8] S. Traiviratana, E.M. Bringa, D.J. Benson, M.A. Meyers, Acta Mater. 56 (15) (2008) 3874, http://dx.doi.org/10.1016/j.actamat.2008.03.047.
[9] E.M. Bringa, S. Traiviratana, M.A. Meyers, Acta Mater. 58 (13) (2010) 4458, http://dx.doi.org/10.1016/j.actamat.2010.04.043.
[10] X. Deng, W. Zhu, Y. Zhang, H. He, F. Jing, Comput. Mater. Sci. 50 (1) (2010) 234, http://dx.doi.org/10.1016/j.commatsci.2010.08.008.
[11] A.S. Pohjonen, F. Djurabekova, K. Nordlund, A. Kuronen, S.P. Fitzgerald, J. Appl. Phys. 110 (2) (2011) 023509, http://dx.doi.org/10.1063/1.3606582.
[12] E.M. Bringa, V.A. Lubarda, M.A. Meyers 63 (1) (2010) 148, http://dx.doi.org/10.1016/j.scriptamat.2010.02.038.
[13] M.A. Meyers, H. Jarmakani, B.Y. Cao, C.T. Wei, B. Kad, B.A. Remington, E.M. Bringa, B. Maddox, D. Kalantar, D. Eder, A. Koniges, vol. 2, EDP Sciences, 2009, p. 999, http://dx.doi.org/10.1051/dymat/2009140.

[14] R.E. Rudd, J.F. Belak, Comput. Mater. Sci. 24 (1–2) (2002) 148, http://dx.doi.org/10.1016/S0927-0256(02)00181-7.
[15] J. Marian, J. Knap, G. Campbell, Acta Mater. 56 (10) (2008) 2389, http://dx.doi.org/10.1016/j.actamat.2008.01.050.
[16] H. Jarmakani, B. Maddox, C. Wei, D. Kalantar, M. Meyers, Acta Mater. 58 (14) (2010) 4604, http://dx.doi.org/10.1016/j.actamat.2010.04.027.
[17] S.-N. Luo, AIP Conf. Proc. 1426 (2012) 1259, http://dx.doi.org/10.1063/1.3686509.
[18] R.F. Zhang, J. Wang, I.J. Beyerlein, T.C. Germann, Philos. Mag. Lett. 91 (12) (2011) 731, http://dx.doi.org/10.1080/09500839.2011.615348.
[19] S.V. Razorenov, G. Garkushin, G.I. Kanel, O.N. Ignatova, AIP Conf. Proc. (2012) 991, http://dx.doi.org/10.1063/1.3686444.
[20] Q. An, R. Ravelo, T.C. Germann, I.W.A. Goddard, AIP Conf. Proc. 1426 (2012) 1259, http://dx.doi.org/10.1063/1.3686509.
[21] K. Kadau, Science 296 (5573) (2002) 1681, http://dx.doi.org/10.1126/science.1070375.
[22] N. Gunkelmann, H. Ledbetter, H.M. Urbassek, Acta Mater. 60 (12) (2012) 4901, http://dx.doi.org/10.1016/j.actamat.2012.05.038.
[23] K. Wang, S. Xiao, M. Liu, H. Deng, W. Zhu, W. Hu, Proc. Eng. 61 (2013) 122, http://dx.doi.org/10.1016/j.proeng.2013.07.104.
[24] H.-S. Park, N. Barton, J.L. Belof, K.J.M. Blobaum, R.M. Cavallo, A.J. Comley, B. Maddox, M.J. May, S.M. Pollaine, S.T. Prisbrey, B. Remington, R.E. Rudd, D.W. Swift, R.J. Wallace, M.J. Wilson, A. Nikroo, E. Giraldez, AIP Conf. Proc. 1426 (2012) 1371, http://dx.doi.org/10.1063/1.3686536.
[25] R.E. Rudd, A.J. Comley, J. Hawreliak, B. Maddox, H.-S. Park, B.A. Remington, AIP Conf. Proc. (2012) 1379, http://dx.doi.org/10.1063/1.3686538.
[26] T.C. Germann, B.L. Holian, P.S. Lomdahl, J.R. Ravelo, Phys. Rev. Lett. 84 (23) (2000) 5351, http://dx.doi.org/10.1103/PhysRevLett.84.5351.
[27] R. Ravelo, T.C. Germann, O. Guerrero, Q. An, B.L. Holian, Phys. Rev. B 88 (2013) 134101, http://dx.doi.org/10.1103/PhysRevB.88.134101.
[28] L. Burakovsky, S.P. Chen, D.L. Preston, A.B. Belonoshko, A. Rosengren, A.S. Mikhaylushkin, S.I. Simak, J.A. Moriarty, Phys. Rev. Lett. 104 (2010) 255702, http://dx.doi.org/10.1103/PhysRevLett.104.255702.
[29] L. Murr, M. Meyers, C.-S. Niou, Y. Chen, S. Pappu, C. Kennedy, Acta Mater. 45 (1) (1997) 157, http://dx.doi.org/10.1016/S1359-6454(96)00145-0.
[30] J.K. Zhou, L.L. Hsiung, R. Chau, C.K. Saw, M. Elert, M.D. Furnish, R. Chau, N. Holmes, J. Nguyen, AIP Conf. Proc. 955 (2007) 677, http://dx.doi.org/10.1063/1.2833192.
[31] C. Lu, B. Remington, B. Maddox, B. Kad, H. Park, S. Prisbrey, M. Meyers, Acta Mater. 60 (19) (2012) 6601, http://dx.doi.org/10.1016/j.actamat.2012.08.026.
[32] A.J. Comley, B.R. Maddox, R.E. Rudd, S.T. Prisbrey, J.A. Hawreliak, D.A. Orlikowski, S.C. Peterson, J.H. Satcher, A.J. Elsholz, H.-S. Park, B.A. Remington, N. Bazin, J.M. Foster, P. Graham, N. Park, P.A. Rosen, S.R. Rothman, A. Higginbotham, M. Suggit, J.S. Wark, Phys. Rev. Lett. 110 (11) (2013) 115501, http://dx.doi.org/10.1103/PhysRevLett.110.115501.
[33] B. Hammel, D. Swift, B. El-Dasher, M. Kumar, G.W. Collins, J. Florando, AIP Conf. Proc. (2012) 931, http://dx.doi.org/10.1063/1.3686430.
[34] J.N. Florando, N.R. Barton, B.S. El-Dasher, J.M. McNaney, M. Kumar, J. Appl. Phys. 113 (8) (2013) 083522, http://dx.doi.org/10.1063/1.4792227.
[35] J.M. McNaney, B. Torralva, K.T. Lorenz, B.A. Remington, M. Wall, M. Kumar, M. Elert, M.D. Furnish, W.W. Anderson, W.G. Proud, W.T. Butler, AIP Conf. Proc (2009) 677, http://dx.doi.org/10.1063/1.3295230.
[36] S. Cuesta-Lopez, J.M. Perlado 60 (2) (2011) 590.
[37] Y. Li, D.J. Siegel, J.B. Adams, X.-Y. Liu, Phys. Rev. B 67 (2003) 125101, http://dx.doi.org/10.1103/PhysRevB.67.125101.
[38] J.-P. Cuq-Lelandais, M. Boustie, L. Soulard, L. Berthe, J. Bontaz-Carion, T. d. Resseguier, AIP Conf. Proc. 1426 (2012) 1167, http://dx.doi.org/10.1063/1.3686487.
[39] R.A. Johnson, D.J. Oh, J. Mater. Res. 4 (05) (1989) 1195, http://dx.doi.org/10.1557/JMR.1989.1195.
[40] S. Plimpton, J. Comp. Phys. 117 (1) (1995) 1, http://dx.doi.org/10.1006/jcph.1995.1039.
[41] L.P. Davila, P. Erhart, E.M. Bringa, M.A. Meyers, V.A. Lubarda, M.S. Schneider, R. Becker, M. Kumar, Appl. Phys. Lett. 86 (16) (2005) 161902, http://dx.doi.org/10.1063/1.1906307.
[42] P. Erhart, E.M. Bringa, M. Kumar, K. Albe, Phys. Rev. B 72 (2005) 052104, http://dx.doi.org/10.1103/PhysRevB.72.052104.
[43] A. Kubota, M.-J. Caturla, S. Payne, T. Diaz de la Rubia, J. Latkowski, J. Nucl. Mater 307–311 (2002) 891, http://dx.doi.org/10.1016/S0022-3115(02)01008-5.
[44] A. Kubota, D.B. Reisman, W.G. Wolfer, Appl. Phys. Lett. 88 (24) (2006) 241924, http://dx.doi.org/10.1063/1.2210799.
[45] R.E. Rudd, Philos. Mag. 89 (34) (2009) 3133, http://dx.doi.org/10.1080/14786430903222529.
[46] Y. Tang, E.M. Bringa, M.A. Meyers, Acta Mater. 60 (12) (2012) 4856, http://dx.doi.org/10.1016/j.actamat.2012.05.030.
[47] C. Ruestes, E. Bringa, A. Stukowski, J. Rodríguez Nieva, G. Bertolino, Y. Tang, M. Meyers, Scr. Mater. 68 (10) (2013) 817, http://dx.doi.org/10.1016/j.scriptamat.2013.01.035.
[48] E.M. Bringa, K. Rosolankova, R.E. Rudd, B.A. Remington, J.S. Wark, M. Duchaineau, D.H. Kalantar, J. Hawreliak, J. Belak, Nat. Mater 5 (10) (2006) 805, http://dx.doi.org/10.1038/nmat1735.
[49] L.M. Dupuy, E.B. Tadmor, R.E. Miller, R. Phillips, Phys. Rev. Lett. 95 (2005) 060202, http://dx.doi.org/10.1103/PhysRevLett.95.060202.
[50] D.R. Tramontina, C.J. Ruestes, Y. Tang, E.M. Bringa, (submitted for publication).
[51] X.D. Dai, Y. Kong, J.H. Li, B.X. Liu, J. Phys.: Condens. Mater. 18 (19) (2006) 4527, http://dx.doi.org/10.1088/0953-8984/18/19/008.
[52] B. Holian, Phys. Rev. A 37 (7) (1988) 2562, http://dx.doi.org/10.1103/PhysRevA.37.2562.
[53] M.M. Budzevich, V.V. Zhakhovsky, C.T. White, I.I. Oleynik, Phys. Rev. Lett. 109 (2012) 125505, http://dx.doi.org/10.1103/PhysRevLett.109.125505.
[54] E.M. Bringa, J.U. Cazamias, P. Erhart, J. Stolken, N. Tanushev, B.D. Wirth, R.E. Rudd, M.J. Caturla, J. Appl. Phys. 96 (7) (2004) 3793, http://dx.doi.org/10.1063/1.1789266.
[55] E.M. Bringa, A. Caro, Y. Wang, M. Victoria, J.M. McNaney, B.A. Remington, R.F. Smith, B.R. Torralva, H.V. Swyngenhoven, Science 309 (5742) (2005) 1838, http://dx.doi.org/10.1126/science.1116723.
[56] M.A. Shehadeh, E.M. Bringa, H.M. Zbib, J.M. McNaney, B.A. Remington, Appl. Phys. Lett. 89 (17) (2006) 171918, http://dx.doi.org/10.1063/1.2364853.
[57] A. Stukowski, K. Albe, Model. Simul. Mater. Sci. Eng. 18 (8) (2010) 085001, http://dx.doi.org/10.1088/0965-0393/18/8/085001.
[58] H. Tsuzuki, P.S. Branicio, J.P. Rino, Comput. Phys. Commun. 177 (6) (2007) 518, http://dx.doi.org/10.1016/j.cpc.2007.05.018.
[59] A. Stukowski, A. Arsenlis, Model. Simul. Mater. Sci. Eng. 20 (3) (2012) 035012, http://dx.doi.org/10.1088/0965-0393/20/3/035012.
[60] R.E. Rudd, Mater. Sci. Forum 633 (2009) 3, http://dx.doi.org/10.4028/www.scientific.net/MSF.633-634.3.
[61] A. Higginbotham, M.J. Suggit, E.M. Bringa, P. Erhart, J.A. Hawreliak, G. Mogni, N. Park, B.A. Remington, J.S. Wark, Phys. Rev. B 88 (2013) 104105, http://dx.doi.org/10.1103/PhysRevB.88.104105.
[62] A. Stukowski, Model. Simul. Mater. Sci. Eng. 18 (1) (2010) 015012, http://dx.doi.org/10.1088/0965-0393/18/1/015012.
[63] W. Humphrey, A. Dalke, K. Schulten, J. Mol. Graph. 14 (1) (1996) 33, http://dx.doi.org/10.1016/0263-7855(96)00018-5.
[64] A.H. Squillacote, J. Ahrens, The ParaView Guide, Kitware, Clifton Park, NY, 2006.
[65] L.L. Hsiung, J. Phys. Condens. Mater. 22 (38) (2010) 385702, http://dx.doi.org/10.1088/0953-8984/22/38/385702.
[66] C. Chen, G. Hu, J. Florando, M. Kumar, K. Hemker, K. Ramesh, Scr. Mater. 69 (10) (2013) 709, http://dx.doi.org/10.1016/j.scriptamat.2013.07.010.
[67] K. Lagerlof, Acta Metall. Mater. 41 (7) (1993) 2143, http://dx.doi.org/10.1016/0956-7151(93)90384-5.
[68] J. Christian, S. Mahajan, Prog. Mater. Sci. 39 (1–2) (1995) 1, http://dx.doi.org/10.1016/0079-6425(94)00007-7.
[69] Y. Zhu, X. Liao, X. Wu, Prog. Mater. Sci. 57 (1) (2012) 1, http://dx.doi.org/10.1016/j.pmatsci.2011.05.001.
[70] Y. Gu, L.-Q. Chen, T.W. Heo, L. Sandoval, J. Belak, Scr. Mater. 68 (7) (2013) 451, http://dx.doi.org/10.1016/j.scriptamat.2012.11.022.
[71] L.A. Sandoval, M.P. Surh, A.A. Chernov, D.F. Richards, J. Appl. Phys. 114 (11) (2013) 113511, http://dx.doi.org/10.1063/1.4821956.
[72] Y. Zhang, P.C. Millett, M. Tonks, S. Biner, Acta Mater. 60 (18) (2012) 6421, http://dx.doi.org/10.1016/j.actamat.2012.08.029.
[73] Y. Tang, E.M. Bringa, M.A. Meyers, Mater. Sci. Eng. A 580 (2013) 414, http://dx.doi.org/10.1016/j.msea.2013.05.024.
[74] J. Hawreliak, H.E. Lorenzana, B.A. Remington, S. Lukezic, J.S. Wark, Rev. Sci. Instum. 78 (2007) 083908, http://dx.doi.org/10.1063/1.2772210.
[75] N.R. Barton, J.V. Bernier, R. Becker, A. Arsenlis, R. Cavallo, J. Marian, M. Rhee, H.-S. Park, B.A. Remington, R.T. Olson, J. Appl. Phys. 109 (7) (2011) 073501, http://dx.doi.org/10.1063/1.3553718.
[76] B. Cao, E.M. Bringa, M.A. Meyers, Metall. Mater. Trans. A 38 (11) (2007) 2681, http://dx.doi.org/10.1007/s11661-007-9248-9.
[77] D.W. Brown, I.J. Beyerlein, T.A. Sisneros, B. Clausen, C.N. Tomé, J. Int. Plast. 29 (2012) 120, http://dx.doi.org/10.1016/j.ijplas.2011.08.006.
[78] R.W. Armstrong, F.J. Zerilli, J. Phys. D 43 (49) (2010) 492002, http://dx.doi.org/10.1088/0022-3727/43/49/492002.
[79] M.J. Suggit, A. Higginbotham, J.A. Hawreliak, G. Mogni, G. Kimminau, P. Dunne, A.J. Comley, N. Park, B.A. Remington, J.S. Wark, Nat. Commun. 3 (2012) 1224, http://dx.doi.org/10.1038/ncomms2225.
[80] M.A. Meyers, B.A. Remington, B. Maddox, E.M. Bringa, JOM 62 (1) (2010) 24, http://dx.doi.org/10.1007/s11837-010-0006-x.